Facile Synthetic Route to a Novel Electroluminescent Polymer−Poly(*p*-phenylenevinylene) Containing a Fully Conjugated Aromatic Oxadiazole Side Chain

Hong Meng, Wang-Lin Yu, and Wei Huang*

Institute of Materials Research and Engineering (IMRE), National University of Singapore, 3 Research Link, Singapore 117602, Republic of Singapore

Received May 12, 1999; Revised Manuscript Received September 21, 1999

ABSTRACT: Herein we report a facile synthetic route to a new conjugated polymer, poly{2-[5′-(2″-octyloxy)phenyl)-1′,3′,4′-oxadiazole-2′-yl]-1,4-phenylenevinylene)} (OPO−PPV), in which a high-electron-affinity aromatic oxadiazole moiety is attached on the PPV backbone as side chain. It is demonstrated that OPO−PPV is a new polymeric material with balanced charge injection for the application as emissive material in single-layer light-emitting diodes (LEDs). The present synthesis of OPO−PPV reveals a promising approach to balance the charge injection between electrons and holes into electroluminescent layers in polymer LEDs by controlling the intrinsic properties of light-emitting materials. The NMR (^{13}C and ^{1}H) spectra of OPO−PPV demonstrate a well-defined structure in the polymer. The polymer exhibits good thermal stability (stable up to 368 °C in nitrogen) and high glass-transition temperature (170 °C). Both the absorption and photoluminescence spectra of the polymer have been studied. Cyclic voltammetry (CV) has been employed to estimate the highest occupied and lowest unoccupied molecular orbital energy levels of OPO−PPV. A comparison of the electrochemical characteristics with that of poly[2-methoxy-5-(2′-ethylhexyloxy)-1,4-phenylenevinylene] (MEH−PPV) is also discussed. A single-layer LED device ITO/OPO−PPV/Al is successfully fabricated. The device emits visible yellow-orange light above the bias voltage of 4.0 V under ambient conditions.

Introduction

In the past decade, because of the discovery of electroluminescence in a conjugated polymer poly(*p*-phenylenevinylene) (PPV), tremendous efforts have been devoted to the design and synthesis of novel polymeric materials with high light emission efficiency for LED applications.[1−4] The high photoluminescence (PL) and electroluminescence (EL) efficiencies, chemically tailorable optical properties, and ease of polymerization of PPV-based polymers have rendered them being strong contenders as emissive materials in polymer LEDs.[5] On the other hand, the realization of new emissive spectra and the improvement for EL performance require the effective and fine control for the energy levels of molecular orbitals of EL polymers. A common problem of PPV-based polymers used in polymer LEDs is poor electron-accepting ability due to their low energy levels (below the vacuum) of the lowest unoccupied molecular orbital (LUMO). Thus, for PPV, electron injection has been proven to be much more difficult than hole injection, resulting in the imbalance of injection between electrons and holes and thus lowering quantum efficiency.[5] Although EL quantum efficiency may be increased greatly by adding charge injection/transporting layers between a light-emitting polymer film and electrodes,[6] the multilayer devices may cause the space-charge and tunneling of accumulated holes and thus damage the devices.[7] Therefore, to improve the device performance, there is still a need to design and synthesize polymeric EL materials with desired highest occupied molecular orbital (HOMO) and LUMO energy levels so that they can match the work functions of the anode and cathode well. Quantum chemical calculations and previous research works have demonstrated that introduction of an electron-withdrawing group onto either the aryl ring or the vinyl group of PPV would lower both the HOMO and LUMO energies of the polymer, thus improving the electron injection.[5,8]

Aromatic oxadiazole-based compounds have high electron affinities, which facilitate both electron injection and transport.[9,10] Polymers containing oxadiazole species have been widely used in electronic devices as electron-transporting and hole-blocking materials.[11] Highly efficient light-emitting diodes based on a PPV derivative carrying 2-(4-biphenyl)-5-(4-*tert*-butylphenyl)-1,3,4-oxadiazole (PBD) have been reported.[12] An oxadiazole ring may be incorporated into backbones to tune the electronic properties of the resulting polymers.[13] Our previous works have demonstrated the effectiveness of *p*−*n* diblock conjugated structures containing oxadiazole moiety in tuning optical and electronic properties of conjugated polymers.[14] A similar approach of copolymerization for tuning the HOMO/LUMO levels of conjugated polymers has also been reported in other conjugated polymer systems.[15,16] Oxadiazole groups are also attached onto conjugated backbones as side chains (groups) to form hybrid polymers.[17] In comparison with main chain (backbone) modifications, the electronic properties of the backbones are less effected by the side chain modifications. In this contribution, we present the synthesis and characterization of a new oxadiazole-containing PPV-based conjugated polymer, in which the oxadiazole ring is attached on PPV backbone as a part of the side chain, but it is also in conjugation with the backbone. The chemical structure of the polymer is illustrated in Figure 1.

* To whom correspondence should be addressed. Fax: (65) 874-8592. E-mail: wei-huang@imre.org.sg.

a

b
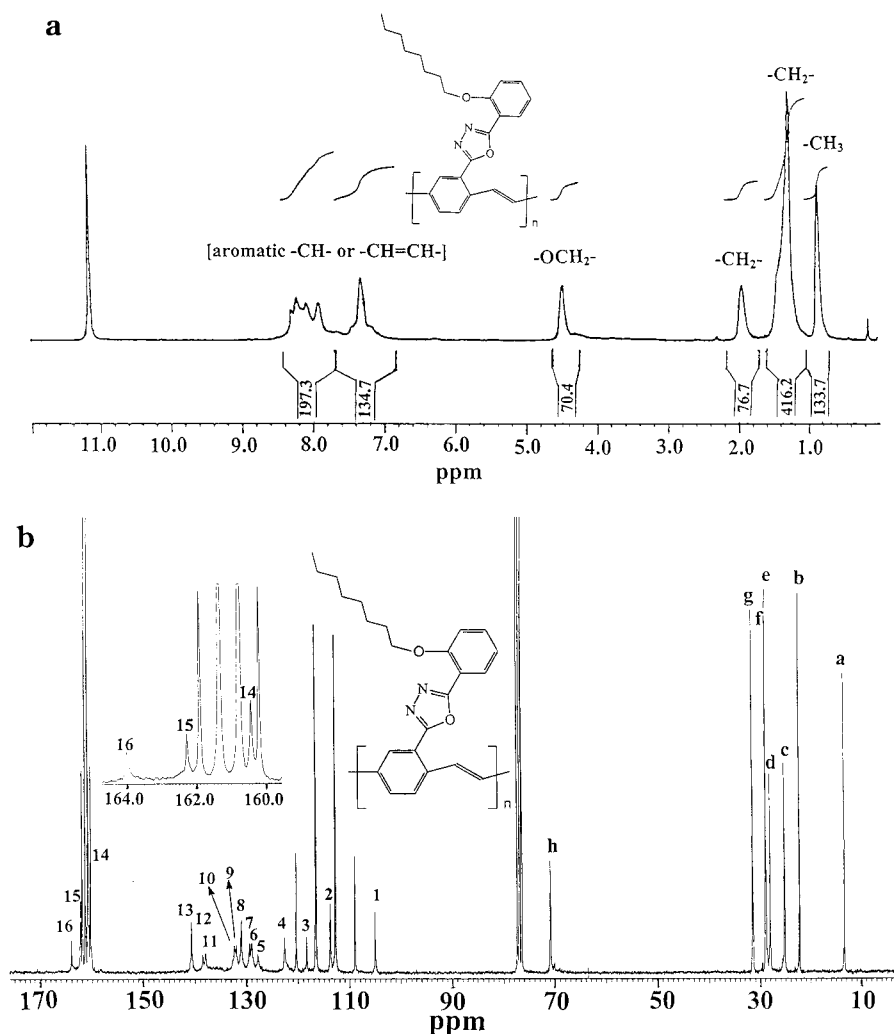
Figure 1. ^{1}H NMR (a) and ^{13}C NMR (b) spectra of OPO–PPV.

Experimental Section

Measurements. NMR spectra were collected on a Bruker ACF 300 spectrometer with chloroform-*d* as solvent and tetramethylsilane as internal standard. FT-IR spectra were recorded on a Bio-Rad FTS 165 spectrometer by dispersing samples in KBr disks. UV–visible and fluorescence spectra were obtained on a Shimadzu UV–NIR 3100 spectrophotometer and on a Perkin-Elmer LS 50B luminescence spectrometer, respectively. Melting points (mp) were measured with an Electrothermal IA 9300 digital melting point apparatus. Thermogravimetric analysis (TGA) was conducted with a Du Pont Thermal Analyst 2100 system with a TGA 2950 thermogravimetric analyzer under a heating rate of 20 °C/min and an air or nitrogen flow rate of 75 mL/min. Differential scanning calorimetry (DSC) was run on a Du Pont DSC 2910 module in conjunction with the Du Pont Thermal Analyst system. Elemental microanalyses were performed on a Perkin-Elmer 240C elemental analyzer for C, H, N and S determinations. Cyclic voltammetry (CV) was performed on an EG&G Parc model 273A potentiostat/galvanostat system with a three-electrode cell in a solution of Bu$_4$NBF$_4$ (0.10 M) in acetonitrile at a scan rate of 50 mV/s. The polymer films were coated on a square Pt electrode (~1.0 cm^2) by dipping the electrode into the corresponding solutions and then drying in air. A Pt wire was used as the counter electrode, and a Ag/AgNO$_3$ (0.10 M) electrode was used as the reference electrode. Gel permeation chromatography (GPC) analysis was conducted with a Waters 2690 separations module equipped with Waters 410 differential refractometer HPLC system with Waters Styragel HR 4E and HR 5E columns using polystyrene as standard and THF as eluant. In the fabrication of single-layer LED device,

indium tin oxide (ITO)-coated glass with a resistivity of 250 Ω/□ was used as substrate. Uniform film (thickness about 1200 Å) of the polymer was obtained by spin coating from the polymer solution dissolved in trifluoroacetic acid (TFA)–CHCl$_3$ (1:5, v/v) at a rate of 5000 rpm for 2 min. The film was dried in a vacuum oven at 30 °C for 24 h before device fabrication. Aluminum was thermally evaporated (JEE–400 vacuum evaporator) as the top electrode at a pressure around 3×10^{-7} Torr, yielding a 1000 Å layer (Thickness Monitor model TM-200R, Maxtek Inc.). An active area of the LED device is about 1 mm^2 as defined by the top electrode. Electrical contacts were fixed using a conductive epoxy 14G adhesive. All the processes except the evaporation of top electrode were done under ambient atmosphere. Electrical and optical characterizations were also carried out under ambient atmosphere. Current–voltage (*I–V*) characteristics were measured with a Keithley 238 high-current source measure unit.

Materials. Diethyl ether was distilled over sodium/benzophenone, and hexane was distilled over calcium hydride. Triethylamine (Aldrich, A. R. grade) was redistilled prior to use. 1-Bromodecane, thionyl chloride, and phosphorusoxachloride were used as received from Aldrich.

Methyl 2-Octoxylbenzoate (1). To the mixture of 50.0 g (0.33 mol) of methyl 2-hydroxybenzoate dissolved in 250 mL of acetone was added 55.2 g (0.40 mol) of potassium carbonate. The reaction was refluxed for 0.5 h, and then 77.2 g (0.40 mol) of 1-octyl bromide was added dropwise over a period of 1 h. The mixture was further refluxed for 48 h. The reaction was then cooled and filtered. The solid was washed with acetone. After removal of the solvent from the combined filtrate, the residue was dissolved in ethyl acetate, washed several times

with 5% KOH and water, and then dried over anhydrous magnesium sulfate. The solvents were removed by rotary evaporation, and the residue was distilled to remove the excess 1-octyl bromide. The residue was purified by vacuum distillation (115 °C/1.5 mmHg) to afford a liquid (66.3 g, yield: 76%). MS: m/z 264. ^{1}H NMR (CDCl$_3$): δ 7.76−7.74 (m, J = 7.9, 1 H), 7.41−7.36 (m, 1 H), 6.94−6.89 (m, 2 H), 4.01−3.98 (t, J = 6.5, 2 H), 3.85 (s, 3 H), 1.82−1.75 (m, 2 H), 1.50−1.27 (m, 10 H), 0.89−0.85 (t, J = 6.5, 3 H) ppm. ^{13}C NMR (CDCl$_3$): δ 166.83, 158.52, 133.14, 131.42, 120.38, 119.81, 113.08, 68.79, 51.65, 31.69, 29.19, 29.13, 29.07, 25.84, 22.53, 13.94 ppm. Anal. Calcd for C$_{16}$H$_{24}$O$_3$: C, 72.69; H, 9.15. Found: C, 72.77; H, 9.33.

2-Octoxylbenzoyl Hydrazine (2). A mixture of 25.0 g (0.095 mol) of methyl 2-octoxybenzoate and 15 g (excess) of hydrazine monohydrate was refluxed for about 3 h. The reaction mixture was cooled and then recrystallized from ethanol to afford 22.2 g (yield: 89%) of white crystal. Mp: 42−43 °C. MS: m/z 264. ^{1}H NMR (CDCl$_3$): δ 9.0 (b, NH, 1 H), 8.21−8.18 (d, J = 7.8, 1 H), 7.45−7.39 (m, J = 7.6, 8.3, 1 H), 7.09−7.04 (m, J = 7.6, 1 H), 6.97−6.94 (d, J = 8.3, 1 H), 4.2−4.1 (b, NH$_2$, 2 H), 4.22−4.18 (t, J = 6.8, 2 H), 1.93−1.79 (m, 2 H), 1.50−1.29 (m, 10 H), 0.91−0.86 (m, 3 H) ppm. ^{13}C NMR (CDCl$_3$): δ 168.41, 158.83, 132.76, 131.92, 120.99, 119.83, 112.10, 69.02, 31.60, 29.09, 29.02, 28.94, 25.91, 22.48, 13.94 ppm. Anal. Calcd for C$_{15}$H$_{24}$N$_2$O$_2$: C, 68.15; H, 9.15; N, 10.60. Found: C, 68.22; H, 9.26; N, 10.58.

2,5-Dimethylbenzoic Acid (3). 2-Bromo-*p*-xylene (37.0 g, 0.20 mol) was reacted with 5.0 g (0.21 mol) of magnesium in 150 mL of anhydrous ether for 1 h, and then the mixture was refluxed for an additional 0.5 h. Subsequently, the reaction mixture was cooled to −70 °C and slowly poured into a 200 mL flask half filled with crushed dry ice under the protection of dry nitrogen. The mixture was warmed to room temperature overnight and then poured into 150 mL of cooled 1 M HCl solution (with ice). The aqueous layer was extracted twice with chloroform. The combined chloroform solutions were washed with water and saturated sodium chloride solution successively and then were dried over anhydrous MgSO$_4$ and filtered. After removal of the solvent and recrystallization from ethanol−water, 23.4 g (78%) of pure product was obtained. Mp: 135−136 °C. MS: m/z 150. ^{1}H NMR (CDCl$_3$): δ 10.5−9.0 (b, 1 H), 7.89 (s, 1 H), 7.28−7.26 (d, J = 6.4, 1 H), 7.18−7.15 (d, J = 6.5, 1 H), 2.62 (s, 3 H), 2.37 (s, 3 H). ^{13}C NMR (CDCl$_3$): δ 173.76, 136.17, 135.32, 133.67, 131.93, 131.78, 128.03, 21.54, 20.64 ppm. Anal. Calcd for C$_9$H$_{10}$O$_2$: C, 71.98; H, 6.71. Found: C, 71.43; H, 6.38.

2,5-Dimethylbenzoyl Chloride (4). Thionyl chloride (100 mL) was added to **3** (20.5 g, 0.137 mol). The mixture was refluxed for 8 h, and then, the excess thionyl chloride was removed under reduced pressure. The residue was distilled under reduced pressure to give 22.1 g of colorless liquid (yield: 96%) (79 °C/0.1 mmHg). MS: m/z 168. ^{1}H NMR (CDCl$_3$): δ 8.02 (s, 1 H), 7.33−7.31 (d, J = 7.7, 1 H), 7.19−7.16 (d, J = 7.7, 1 H), 2.52 (s, 3 H), 2.40 (s, 3 H) ppm. ^{13}C NMR (CDCl$_3$): δ 167.36, 138.24, 138.05, 134.92, 134.20, 132.03, 131.75, 21.41, 20.73 ppm. Anal. Calcd for C$_9$H$_9$OCl: C, 64.11; H, 5.38; Cl, 21.03. Found: C, 63.98; H, 5.27; Cl, 21.12.

***N*-(2,5-Dimethylbenzoyl)-*N*′-(2-octoxylbenzoyl)hydrazine (5).** 2,5-Dimethylbenzoyl chloride (**4**) (8.50 g, 0.05 mol) was added into a solution containing 13.32 g (0.05 mol) of **2** and 5.01 g (0.05 mol) of triethylamine in 200 mL of CH$_2$Cl$_2$ under vigorous stirring. The reaction mixture was further stirred for about 2 h and then washed with water three times. The organic layer was dried over anhydrous MgSO$_4$. The solution was filtered and concentrated, and the resulting solid was recrystallized from ethanol/water to yield 19.2 g (97%) of white crystals. Mp: 94−95 °C. MS: m/z 396. ^{1}H NMR (CDCl$_3$): δ 11.15−11.13 (d, J = 7.7, NH, 1 H), 9.38−9.36 (d, J = 7.7, NH, 1 H), 8.13−8.11 (d, J = 7.3, 1 H), 7.51−7.50 (d, J = 7.3, 1 H), 7.35 (s, 1 H), 7.15 (s, 1 H), 7.14 (s, 1 H), 7.12−7.09 (d, J = 7.3, 1 H), 7.04−7.00 (m, 1 H), 4.24−4.19 (t, J = 6.6, 2 H), 2.47 (s, 1 H), 2.32 (s, 1 H), 2.12−2.05 (m, 2 H), 1.63−1.29 (m, 10 H), 0.89−0.85 (m, 3 H) ppm. ^{13}C NMR (CDCl$_3$) δ: 164.73,

159.88, 157.09, 135.14, 133.71, 133.26, 132.81, 131.92, 131.04, 130.80, 128.18, 120.92, 118.56, 111.93, 69.59, 31.72, 29.19, 28.96, 26.21, 22.55, 20.51, 19.27, 13.98 ppm. Anal. Calcd for C$_{24}$H$_{32}$N$_2$O$_3$: C, 72.70; H, 8.13; N, 7.06. Found: C, 72.97; H, 8.16; N, 7.12.

2-{5′-[(2″-octoxyl)phenyl](1′,3′,4′-oxadiazolyl)}-*para*-xylene (6).[14] **5** (15.0 g, 0.038 mol) was refluxed in 100 mL of POCl$_3$ under nitrogen atmosphere for 8 h. After about 60 mL of POCl$_3$ was distilled off, the reaction mixture was cooled to 50 °C and then poured into 200 mL of water containing ice. The white precipitate was collected by filtration and washed with water. Recrystallization from ethanol afforded 12.8 g of white crystals (yield: 90%). Mp: 75−76 °C. MS: m/z 378. ^{1}H NMR (CDCl$_3$): 8.09−8.06 (d, J = 7.8, 1 H), 7.86 (s, 1 H), 7.46−7.44 (d, J = 7.9, 1 H), 7.26 (s, 1 H), 7.24 (s, 1 H), 7.08−7.07 (m, 1 H), 7.04−7.00 (m, 1 H), 4.14−4.10 (t, J = 6.6, 2 H), 2.73 (s, 1 H), 2.40 (s, 1 H), 1.92−1.87 (m, 2 H), 1.69−1.23 (m, 10 H), 0.87−0.83 (m, 3 H) ppm. ^{13}C NMR (CDCl$_3$): δ 164.92, 163.21, 157.26, 135.48, 135.17, 132.81, 131.67, 131.51, 130.54, 129.30, 122.98, 120.48, 113.26, 112.71, 68.78, 31.68, 29.24, 29.19, 29.06, 25.89, 22.50, 21.49, 20.74, 13.94 ppm. Anal. Calcd for C$_{24}$H$_{30}$N$_2$O$_2$: C, 76.16; H, 7.99; N, 7.40. Found: C, 75.40; H, 8.04; N, 7.54.

1,4-Bis(bromomethyl)-2-{5′-[(2″-octoxylphenyl)]-1′,3′,4′-oxadiazolyl}benzene (7). **5** (4.36 g, 0.012 mol), 4.10 g (0.011 mol) of *N*-bromosuccinimide (NBS), and a catalytic amount of benzoyl peroxide were dispersed in 80 mL of benzene. The reaction mixture was refluxed for 3 h under nitrogen atmosphere while being exposed to tungsten light. The reaction mixture was extracted three times with water, and then, the organic layer was dried over anhydrous MgSO$_4$. The solution was filtered and concentrated, and the resulting solid was recrystallized from absolute ethanol to afford white crystals in 45% yield. Mp: 121−123 °C. MS: m/z 536. ^{1}H NMR (CDCl$_3$): 8.13 (s, 1 H), 8.12−8.10 (d, J = 7.8, 1 H), 8.09 (s, 1 H), 7.61−7.56 (d, J = 7.0, 1 H), 7.54−7.51 (m, 1 H), 7.48−7.11 (m, 1 H), 7.09−7.06 (m, 1 H), 5.20 (s, 1 H), 4.52 (s, 1 H), 4.16−4.12 (t, J = 6.8, 2 H), 1.96−1.91 (m, 2 H), 1.53−1.24 (m, 10 H), 0.87−0.83 (m, 3 H) ppm. ^{13}C NMR (CDCl$_3$): δ 163.65, 162.90, 157.35, 138.59, 137.42, 133.22, 132.48, 131.73, 130.65, 129.67, 123.14, 120.58, 112.78, 112.72, 68.80, 31.67, 31.56, 31.08, 29.20, 29.15, 29.12, 28.83, 25.85, 22.88, 22.52, 13.98 ppm. Anal. Calcd for C$_{24}$H$_{28}$Br$_2$N$_2$O$_2$: C, 53.75; H, 5.26; Br, 29.80; N, 5.22. Found: C, 53.62; H, 5.54; Br, 28.89; N, 5.28.

Polymerization.[18] **7** (0.436 g, 1.0 mmol) was dissolved in 30 mL of anhydrous THF. To this stirred solution was added dropwise 4.0 mL of a 1.0 M solution of potassium *tert*-butoxide (4.0 mmol) in anhydrous THF at room temperature. The mixture was stirred at ambient temperature for 8 h. The reaction mixture was then poured into 200 mL of stirred methanol. The resulting orange-yellow precipitate was collected by filtration and was washed with methanol and acetone. The solid powder was extracted with chloroform overnight. After removal of the solvent, the final polymer was dried under vacuum to afford 0.187 g (yield: 43%) of an orange-yellow powder. ^{1}H NMR (CDCl$_3$/TFA-*d*): 8.29−7.90 (b, 5 H), 7.33−7.29 (b, 4 H), 4.48 (b, 2 H), 1.95 (b, 2 H), 1.5−1.2 (b, 10 H), 0.9−0.8 (b, 3 H) ppm. ^{13}C NMR (CDCl$_3$/TFA-*d*): δ 164.00, 162.28, 160.42, 140.64, 138.47, 137.93, 132.32, 131.95, 130.98, 129.40, 128.94, 127.78, 122.61, 118.30, 113.78, 105.03 ppm. Anal. Calcd for C$_{22}$H$_{25}$BrN$_2$O$_2$: C, 61.54; H, 5.87; Br, 18.61; N, 6.52. Found: C, 61.63; H, 5.84; Br, 18.39; N, 6.72.

Results and Discussion

Monomer and Polymer Synthesis. There have been a few approaches for introducing aromatic oxadiazole moieties into the polymer side chain to form a fully conjugated polymer. The approaches include the palladium-catalyzed coupling reaction of phenylboronic acid with haloarenes[19] and the one that we recently reported, which is through a nickel-catalyzed Grignard coupling reaction between a bromo-substituted oxadiazole and a bromo-substituted phenylene to form the

Scheme 1. Synthetic Route to OPO−PPV

Figure 2. Thermal analyses of OPO−PPV. TGA chart (a) and DSC curve (b) in nitrogen.
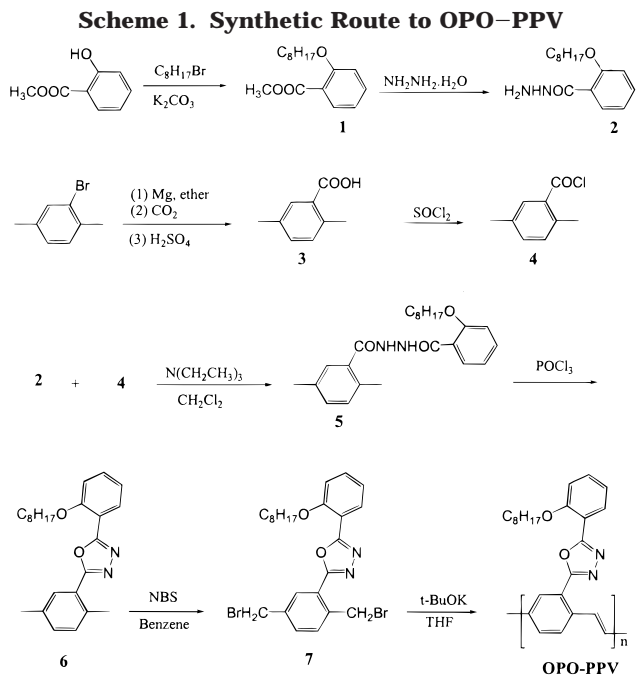
corresponding monomer.[20] These approaches, however, involve several synthetic steps and generally give low yields (∼20%) in the synthesis of monomers. Our new approach is to introduce the oxadiazole ring into the monomer by the reaction between a benzoyl chloride (**4**) and a benzoyl hydrazine (**2**), followed by a cyclodehydrating reaction (see Scheme 1). The benzoyl chloride (**4**) was synthesized from 2-bromo-*para*-xylene through its Grignard reagent to form the acid and a following reaction with thionyl chloride. This method not only gives a high yield (>80%) of the final monomer but also avoids multistep syntheses. The monomer can be easily polymerized in the potassium *tert*-butoxide/THF system with the standard Gilch method. The obtained polymer can be dissolved in $CHCl_3$ and THF. GPC analysis (polystyrene as the standard for calibration) reveals that the number-average molecular weight (M_n) and weight-average molecular weight (M_w) of the polymer are 20 272 and 55 225, respectively, with a polydispersity index of 2.72. Although the molecular weights are generally overestimated by the calibration of polystyrene standards owing to the stiffness of the conjugated polymers, such as PPV derivatives, the results indicate a relatively high molecular weight of the new polymer.

NMR Spectroscopy Characterization. The structure and purity of both monomer and polymer were fully analyzed by FT-IR, ^{1}H and ^{13}C NMR spectra, and elemental analysis. The ^{1}H and ^{13}C NMR spectra were obtained in $CDCl_3$-TFA-*d* (5:1, v/v) solution of the polymer. All chemical shift values are referenced to tetramethylsilane (TMS, 0 ppm). The ^{1}H and ^{13}C NMR spectra of the polymer are depicted in Figure 1. The ^{1}H NMR spectrum of the polymer exhibits the chemical shift of alkyl side chains at 0.83−1.95 ppm. The methyleneoxy protons ($-OCH_2-$) appear at 4.48 ppm, and the vinyl protons adjacent to the phenyl rings and the aromatic phenyl protons are found in the range of 7.2−8.4 ppm. The ^{13}C NMR spectrum indicates that there are 16 (refer to Figure 1, peaks 1−16) different carbons in the low-field region assigned to the 14 aromatic carbons and 2 vinylene carbons. The eight peaks (refer to Figure 1, peaks a−h) located in the high-field region are assigned to the methyl and methylene groups of the
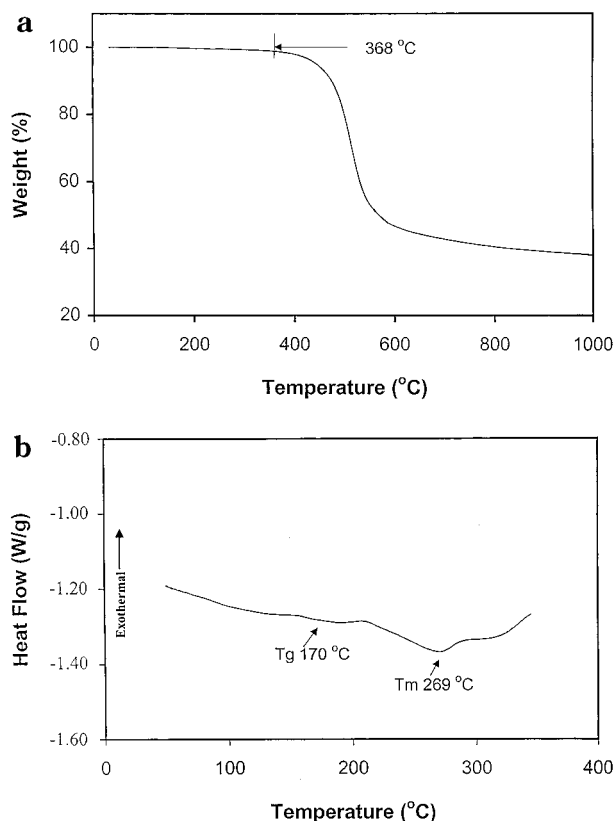
long alkoxy chains, respectively. The NMR spectra agree very well with the polymer structure of poly{2-[5′-(2′′-octyloxyphenyl)-1′,3′,4′-oxadiazole-2′-yl]-1,4-phenylenevinylene} (OPO−PPV). Detailed assignment of the
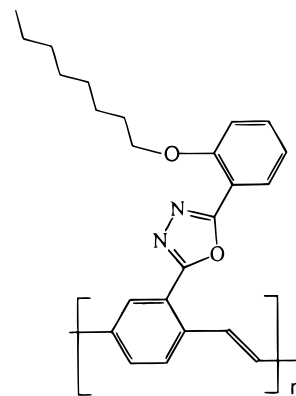
chemical shifts of the NMR (^{13}C and ^{1}H) spectra is difficult because the broadened spectrum of the ^{1}H NMR makes it very complicated. However, there are no peaks due to impurities.

Thermal Analysis of the Polymer. Thermal stability of polymer is important for device longevity. Figure 2a displays the TGA chart of the polymer OPO−PPV. The TGA analysis reveals that the polymer is stable in nitrogen up to 368 °C. Between 368 and 600 °C, there is about 60% weight loss, which is a result of the decomposition of the polymer. Glass-transition (T_g) and melting temperatures of the polymer were determined by differential scanning calorimetry (DSC) in nitrogen atmosphere at a heating rate of 20 °C/min (refer to Figure 2b). The polymer demonstrates the glass-transi-
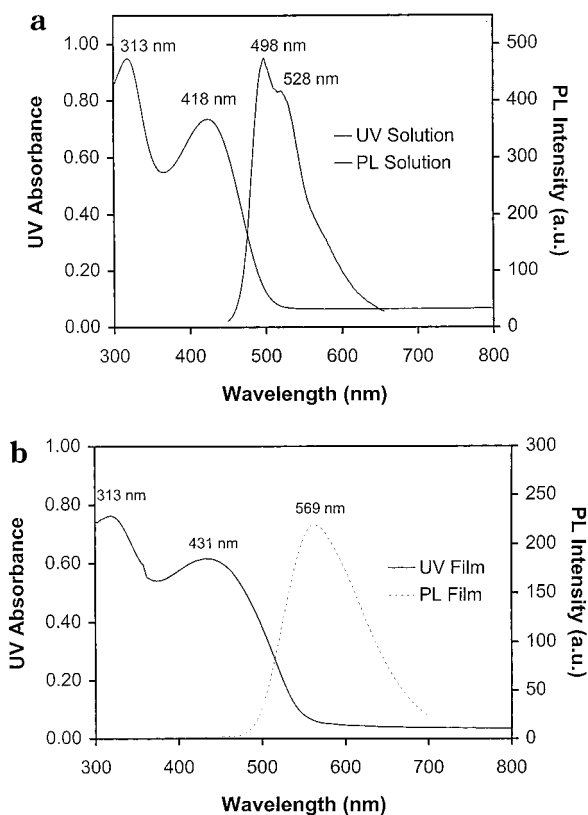
Figure 3. UV−visible absorption and PL (excited at 431 nm) spectra of OPO−PPV in CHCl₃ solution (a) and film states (b) at room temperature.

Figure 4. Cyclic voltammograms of OPO−PPV as films on a Pt electrode in CH₃CN solution of Bu₄NBF₄ (0.10 M) at a scan rate of 50 mV/s.

tion temperature at 170 °C and exhibits melting endotherm at 269 °C. The DSC results indicate that the polymer possesses a high T_g due to the oxadiazole rigid structure, which is an advantage for the lifetime of device. It is said that active emissive polymers and charge injecting/transporting materials with high glass-transition temperature might exhibit longer device lifetime.[21]

UV−Visible and PL Spectra. The UV−visible absorption and photoluminescence (PL) spectra of the polymer are depicted in Figure 3. The UV−visible absorption spectra of the polymer in both solution and neat film show two peaks at 313 and 418 nm and 313 and 431 nm, respectively. The longer wavelength peak in the region of 380−500 nm is attributed to the $\pi-\pi^*$ absorption of the conjugated polymer main chain, whereas the shorter wavelength peak at 313 nm originates from the aromatic side chain. It is interesting to note that the shorter wavelength peaks for the solution and film samples are the same, whereas the $\pi-\pi^*$ absorption peak is redshifted by 13 nm from solution to film. The results imply that the configuration of the side chain is not affected by the variation of state of the polymer, although the main chain of the polymer corresponds to a higher orientation in film states. The absorption edge for the film sample is measured to be 547 nm, from which the $\pi-\pi^*$ band gap energy is estimated to be 2.27 eV. The maximum emission peak of the polymer film, excited at 431 nm, is 569 nm, which corresponds to orange-yellow light.

Cyclic Voltammetry of the Polymer. Cyclic voltammetry (CV) was employed to investigate the redox behavior of the polymer OPO−PPV and to estimate the HOMO and LUMO energy levels of the polymer.[22] As a comparison, MEH−PPV was synthesized and its elec-

trochemical behavior was investigated under the same conditions. The polymer films dip-coated on a Pt electrode were scanned positively and negatively separately in a 0.10 M tetrabutylammonium tetrafluoroborate (Bu₄NBF₄) solution in anhydrous acetonitrile. Figure 4 depicts the CV curves of both the *p*- and *n*-doping processes of the polymer. During the cathodical scan, the film of the polymer OPO−PPV exhibits a reversible *n*-doping process. An incomplete reduction peak appeared at −1.75 V (vs SCE) with the corresponding reoxidation peak at −1.48 V (vs SCE). The onset potential of the reduction is −1.24 V (vs SCE). The reduction potential is comparable with those of the typical electron-transporting/hole-blocking materials. In the anodical scan, a prominent oxidation peak appeared at 1.35 V (vs SCE). The reversibility of the oxidation process is poor; only a very weak rereduction peak was observed around 1.29 V (vs SCE). The onset for the oxidation is determined to be 1.07 V. The polymer films on Pt were stable in the electrochemical reduction and oxidation processes. There was no obvious change in the feature of CV curves during multiscans. The reduction of the polymer film was accompanied by the change in color from greenish-yellow to blue. During the oxidation process, the film color changed first from greenish-yellow to dark blue and then to transparent. From the difference of onset potential between the reduction and oxidation processes, the band gap of the polymer can be estimated to be 2.31 eV, which is close to that obtained from the absorption edge in the UV−visible spectra (2.27 eV).

The CV curves of MEH−PPV are also depicted for comparison. Both *n*- and *p*-doping processes are reversible. Similar to OPO−PPV, there are obvious color changes during the cyclic scans. The color of MEH−PPV

film changes first from red to bluish-brown and then to transparent and back to red in both the cathodically and anodically scanning processes. The onset potentials and the oxidation/reduction peaks of MEH−PPV are indicated in Figure 4b.

The onset potentials of the n- and p-doping processes of a conjugate polymer can be utilized as a surrogate to estimate the HOMO and LUMO energy levels of the polymer.[9] According to the empirical equation reported by deLeeuw et al.,[23] $E_{LUMO} = E_{onset(red)} + 4.4$ eV and $E_{HOMO} = E_{onset(ox)} + 4.4$ eV, where $E_{onset(ox)}$ and $E_{onset(red)}$ are the onset potentials for the oxidation and reduction processes of a polymer vs SCE, respectively. The LUMO energy of the polymer is thus estimated to be 3.16 eV. This value is almost the same as those of some poly-(aromatic oxadiazole)s.[24] The fact implies that the polymer may have electron-injection properties similar to those typical of oxadiazole-containing electron-transporting materials when it is used as the emitter in PLEDs. The LUMO energy level of 3.16 eV is comparable with that of CN−PPV (3.02 eV) and is much better than that of MEH−PPV (2.73 eV).[24] The HOMO energy level can be estimated to be 5.47 eV, which is also lower than that of MEH−PPV (4.96 eV).

The preliminary cyclic voltammetry results show that both the HOMO and LUMO energy levels of the new polymer are lowered by 0.51 and 0.43 eV, respectively, compared with those of MEH−PPV. These energy levels provide a closer match to the work functions of indium−tin oxide (ITO) and Al. The relative barrier energies for the injections of electrons and holes in a single-layered LED device with the configuration of ITO/polymer/Al may be estimated from the HOMO and LUMO energy levels of the polymer and the work functions of the electrodes. The work function of ITO is about 4.7 eV, and the value for Al is 4.2 eV. The barrier energy for the hole injection from ITO to OPO−PPV, ΔE_H, is thus to be estimated as $\Delta E_H = E_{HOMO} - 4.7 = 5.47 - 4.7 = 0.77$ (eV). Similarly, the barrier energy for the electron injection from Al to OPO−PPV, ΔE_E, can be estimated to be $\Delta E_E = 4.2 - E_{LUMO} = 4.2 - 3.16 = 1.04$ (eV). The difference of barrier energy between the electron injection and hole injection is 0.27 eV. If the polymer OPO−PPV is replaced with MEH−PPV, the corresponding ΔE_H and ΔE_E are calculated to be 0.26 and 1.47 eV, respectively. In this case, the difference of barrier energy between electron injection and hole injection is as large as 1.21 eV. The difference of barrier energy between electron injection and hole injection in the device of ITO/polymer/Al is significantly lower for OPO−PPV than that for MEH−PPV. We may conclude that, by the introduction of the electron-withdrawing group of oxadiazole moiety in the PPV side chain, the charge injection balance between holes and electrons in single-layered LED devices using Al as cathodes is improved.

LED Device Strategy. An ITO/OPO−PPV/Al single-layer light-emitting diode was successfully fabricated. The polymer was deposited onto ITO-coated glass substrates by spin-casting the polymer solution in $CHCl_3$. The uniform polymer film was obtained with thickness of about 120 nm. Aluminum was thermally evaporated onto the polymer film as top electrode. Under a forward bias (ITO wired positively), the single-layer diode begins to emit visible yellowish-orange light at about 4 V. The current−voltage (I−V) curve of the ITO/OPO−PPV/Al device, displayed in Figure 5, shows typical diode characteristics. When the forward bias is
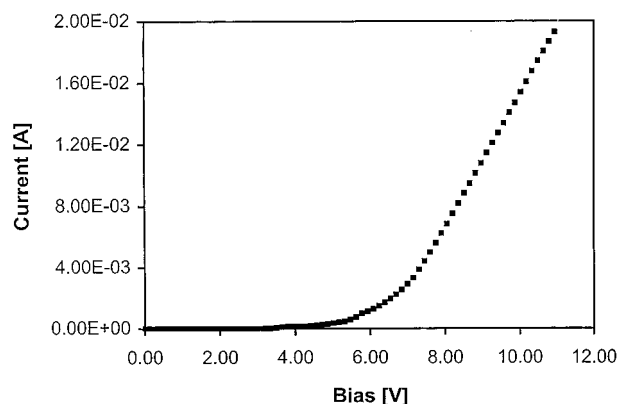
Figure 5. Characteristics of current vs bias of an ITO/OPO−PPV/Al device.
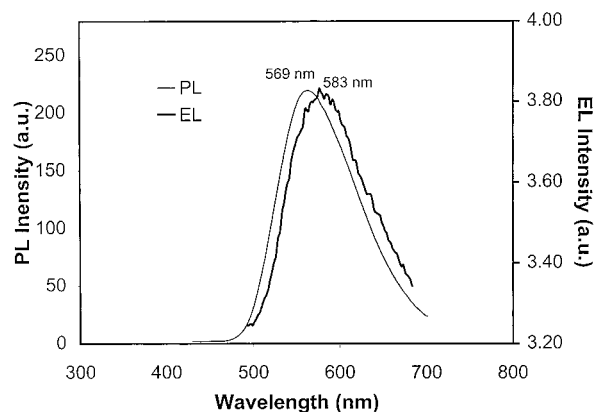
Figure 6. Photoluminescence (PL) and electroluminescence (EL) spectra of OPO−PPV.

increased, the current increases rapidly after 6 V. The EL emission spectrum (see Figure 6) of the polymer is slightly redshifted from its PL spectrum. This may be caused by the interface effect in devices.

The results demonstrate that the new polymer may be a potential active material for use in LEDs. Because the fabrication and characterization of the LED devices were conducted under ambient conditions, better EL performance may be expected if the processes are carried out in more strict conditions. More detailed studies on EL properties of the new polymer is in progress.

Conclusions

A new polymer incorporating an oxadiazole moiety as a fully conjugated side chain to PPV backbone has been successfully synthesized by a facile synthetic route. High-quality polymer films can be easily fabricated by spin-coating techniques because the polymer can be dissolved in common solvents. TGA analysis shows that the polymer has quite good thermal stability, whereas DSC analysis reveals that the polymer possesses a high T_g, which could be valuable for longer device operation when it is used as emission material. The absorption and fluorescent emission spectra of the polymer indicate that it is a yellowish-orange emitting material with a band gap of 2.27 eV. UV−vis spectra shows two peaks that correspond to the $\pi-\pi^*$ transitions of the conjugated polymer backbone and its aromatic oxadiazole side chains. Electrochemical behavior of the copolymer demonstrates that the polymer has much better charge balance injection ability than MEH−PPV. Introducing

the high-electron-affinity oxadiazole moiety into the PPV backbone lowers both the HOMO and LUMO energy levels of the polymer, thus mitigating the problem of the charge imbalance in polymer LEDs. The single-layer LED device with a stable metal (Al) as cathode was successfully fabricated. The threshold voltage of the device is about 4 V, showing the promise of the new polymer as candidate of EL material.

References and Notes

(1) Burroughes, J. H.; Bradley, D. D. C.; Brown, A. R.; Marks, R. N.; MacKay, K.; Friend, R. H.; Burn, P. L.; Holmes, A. B. *Nature* **1990**, *347*, 539−541.

(2) Gustafsson, G.; Cao, Y.; Treacy, G. M.; Klavetter, F.; Colaneri, N.; Heeger, A. J. *Nature* **1992**, *357*, 477−479.

(3) Friend, R. H.; Gymer, R. W.; Holmes, A. B.; Burroughes, J. H.; Marks, R. N.; Taliani, C.; Bradley, D. D. C.; Dos Santos, D. A.; Brédas, J. L.; Lögdlund, M.; Salaneck, W. R. *Nature* **1999**, *397*, 121−128.

(4) (a) Kraft, A.; Grimsdale, A. C.; Holmes, A. B. *Angew. Chem., Int. Ed. Engl.* **1998**, *37*, 402−428. (b) Hide, F.; Diaz-Garcia, M. A.; Achwartz, B. J.; Heeger, A. J. *Acc. Chem. Res.* **1997**, *30*, 430−436. (c) Segura, J. L. *Acta Polym.* **1998**, *49*, 319−344.

(5) Greenham, N. C.; Moratti, S. C.; Bradley, D. D. C.; Friend, R. H.; Holmes, A. B. *Nature* **1993**, *365*, 628−630.

(6) (a) Brown, A. R.; Bradley, D. D. C.; Burroughes, J. H.; Friend, R. H.; Greenham, N. C.; Burn, P. L.; Holmes, A. B.; Kraft, A. *Appl. Phys. Lett.* **1992**, *61*, 2793−2795. (b) Birgerson, J.; Fahlman, M.; Bröms, P.; Salaneck, W. R.; *Synth. Met.* **1996**, *80*, 125−130. (c) Parker, I. D. *J. Appl. Phys.* **1994**, *75*, 1656−1666.

(7) Heischkel, Y.; Schmidt, H. W. *Macromol. Chem. Phys.* **1998**, *199*, 869−880.

(8) (a) Greenham, N. C.; Friend, R. H.; Bradley, D. D. C. *Adv. Mater.* **1994**, *6*, 491−493. (b) Cornil, J.; Beljonne, D.; Dos Santos, D. A.; Brédas, J. L. *Synth. Met.* **1996**, *76*, 101−104.

(9) Strukelj, M.; Papadimitrakopoulos, F.; Miller, T. M.; Rothberg, L. J. *Science* **1995**, *267*, 1969−1972.

(10) Schulz, B.; Bruma, M.; Brehmer, L. *Adv. Mater.* **1997**, *9*, 601−613.

(11) Yang, Y.; Pei, Q. *J. Appl. Phys.* **1995**, *77*, 4807−4809.

(12) Kido, J.; Ohtaki, C.; Hongawa, K.; Okuyama, K.; Nagai, K. *Jpn. J. Appl. Phys.* **1993**, *32*, L917−920.

(13) Peng, Z.; Bao, Z.; Galvin, M. E. *Chem. Mater.* **1998**, *10*, 2086−2090.

(14) (a) Yu, W.-L.; Meng, H.; Pei, J.; Huang, W.; Li, Y.; Heeger, A. J. *Macromolecules* **1998**, *31*, 4838−4844. (b) Yu, W.-L.; Meng, H.; Pei, J.; Huang, W. *J. Am. Chem. Soc.* **1998**, *120*, 11808−11809. (c) Yu, W.-L.; Meng, H.; Pei, J.; Lai, Y.-H.; Chua, S.-J.; Huang, W. *Chem. Commun.* **1998**, 1957−1958. (d) Huang, W.; Meng, H.; Yu, W.-L.; Pei, J.; Chen, Z.-K.; Lai, Y.-H. *Macromolecules* **1999**, *32*, 118−126.

(15) Barbarella, G.; Favaretto, L.; Zambianchi, M.; Pudova, O.; Arbizzani, C.; Bongini, A.; Mastragostino, M. *Adv. Mater.* **1998**, *10*, 551−554.

(16) Redecker, M.; Bradley, D. D. C.; Indasekaran, M.; Wu, W. W.; Woo, E. P. *Adv. Mater.* **1999**, *11*, 241−246.

(17) Bao, Z.; Peng, Z.; Galvin, M. E.; Chandross, E. A. *Chem. Mater.* **1998**, *10*, 1201−1204.

(18) Kang, I.; Hwang, D.; Shim, H.; Zyung, T.; Kim, J. *Macromolecules* **1996**, *29*, 165−169.

(19) Chung, S. J.; Kwon, K. Y.; Lee, S. W.; Jin, J. I.; Lee, C. H.; Lee, C. E.; Park, Y. *Adv. Mater.* **1998**, *10*, 1112−1116.

(20) Chen, Z.-K.; Meng, H.; Lai, Y.-H.; Huang, W. *Macromolecules* **1999**, *32*, 4351−4358.

(21) Fink, R.; Heischkel, Y.; Thelakkat, M.; Schmidt, H. *Chem. Mater.* **1998**, *10*, 3620−3625.

(22) Rusling, J. F.; Suib, S. L. *Adv. Mater.* **1994**, *6*, 922−930.

(23) Leeuw, D. M.; Simenon, M. M.; Brown, A. R.; Einerhand, R. E. F. *Synth. Met.* **1997**, *87*, 53.

(24) Cervini, R.; Li, X.; Spencer, G. W. C.; Holmes, A. B.; Moratti, S. C.; Friend, R. H. *Synth. Met.* **1997**, *84*, 359−360.